Soft Matter

Responsive Blends of Block Copolymers Stabilize the Hexagonally Perforated Lamellae Morphology

Journal:	*Soft Matter*
Manuscript ID	SM-ART-02-2023-000142.R1
Article Type:	Paper
Date Submitted by the Author:	14-Mar-2023
Complete List of Authors:	Nowak, Samantha; Brookhaven National Laboratory, Center for Functional Nanomaterials Tiwale, Nikhil; Brookhaven National Laboratory, Center for Functional Nanomaterials Doerk, Gregory; Brookhaven National Laboratory, Center for Functional Nanomaterials Nam, Chang-Yong; Brookhaven National Laboratory, Center for Functional Nanomaterials; Stony Brook University, Department of Material Science and Chemical Engineering Black, Charles T.; Brookhaven National Laboratory, Center for Functional Nanomaterials Yager, Kevin; Brookhaven National Laboratory, Center for Functional Nanomaterials

SCHOLARONE™
Manuscripts

Responsive Blends of Block Copolymers Stabilize the Hexagonally Perforated Lamellae Morphology

Samantha R. Nowak, Nikhil Tiwale, Gregory S. Doerk, Chang-Yong Nam, Charles T. Black, Kevin G. Yager*

Center for Functional Nanomaterials, Brookhaven National Laboratory, Upton, New York 11973, United States

*email: kyager@bnl.gov

Abstract

Blends of block copolymers can form phases and exhibit features distinct from the constituent materials. We study thin film blends of cylinder-forming and lamellar-forming block copolymers across a range of substrate surface energies. Blend materials are responsive to interfacial energy, allowing selection of pure or coexisting phases based on surface chemistry. Blending stabilizes certain motifs that are typically metastable, and can be used to generate pure hexagonally perforated lamellar thin films across a range of film thicknesses and surface energies. This tolerant behavior is ascribed to the ability of blend materials to redistribute chains to stabilize otherwise high-energy defect structures. The blend responsiveness allows the morphology to be spatially defined through multi-tone chemical surface patterns.

Introduction

Block copolymers (BCP) are a well-studied class of self-assembling materials,[1, 2] where frustrated phase separation generates a nanoscale morphology. If the constituent chains are relatively monodisperse, ordered phases with well-defined symmetry and repeat-spacing (L_0) are formed. In diblock copolymers, the most accessible phases are alternating lamellae (for symmetric chains with equal volume fraction of blocks) and hexagonally-packed cylinders (for asymmetric chains). This straightforward means of accessing ordered nanopatterns in bulk and in thin films[3, 4] has spawned a host of functional material applications.[5-12] There is strong interest in developing methods to form target morphologies beyond those seen in the equilibrium phase diagram of diblock BCPs.[2, 13-19] Synthesis of more complex block architectures is a powerful method for increasing structural diversity, since chain architecture dictates the equilibrium phase diagram.[20-25] Self-assembly is intrinsically responsive to external fields and processing history;[26-29] thus considerable research has gone into directing the assembly of existing diblock copolymers using processing history,[4, 30, 31] solvent exposure,[32, 33] substrate chemistry,[34-36] topographic[37, 38] or chemical[39, 40] patterns, shear forces,[41-45] or thermal fields.[46-48]

The hexagonally perforated lamellar (HPL) phase provides an instructive example of a self-assembled morphology that is difficult to obtain from a simple diblock copolymer.[49-56] In the bulk, these phases are long-lived non-equilibrium states[23] that can only be accessed by, for example, careful control of temperature ramp rate across phase boundaries.[53, 54] Thin films of cylinder-forming BCPs can convert into HPL phases when confined to an appropriate thickness;[56, 57] solvent annealing can be used to promote the transition.[58, 59] The appearance of HPL arises from an interplay between confinement and surface fields.[60-62] Interfacial wetting and thin film confinement impose boundary conditions to which the hexagonally-packed cylinder

unit cell must distort to accommodate; when the distortion energy is sufficiently large, the system may convert into a metastable morphology such as HPL.[63] These HPL phases are often contaminated by the appearance of equilibrium cylinder domains. This highlights a general challenge in forming non-equilibrium phases: metastable states exist in poorly behaved parts of the energy landscape, featuring multiple competing states with low barriers to interconversion. It is thus valuable to investigate strategies for stabilizing otherwise unstable structural motifs.

Blending block copolymers with homopolymers or other block copolymers can be used to tailor material properties. Homopolymer additives can accelerate ordering kinetics,[64, 65] modify the BCP repeat-spacing,[66-68] and induce transitions into other phases.[69] In the bulk, blending of different BCPs may give rise to segregated domains[70-72] and phase coexistence,[55, 73] or homogeneous domains exhibiting a compromise morphology[71, 74-78] which may differ from the pure components.[79, 80] Blending in the bulk has proven to be a viable means of engineering the morphology,[81-83] since the mixture of chains can redistribute to stabilize what would otherwise be high-energy structural motifs. In thin films, blends can exhibit coexistence phases,[84, 85] and chemical gratings can be used to select which phase forms.[86] Average surface chemistry influences the orientation[36, 87, 88] and feature size[89] of single-component BCP films.

Here, we study thin film blends of cylinder and lamellar-forming BCPs, and identify a broad region where a homogeneous HPL phase is formed. We find that blending makes this phase more robust (e.g., tolerant to casting conditions). These observations can be ascribed to stabilization of the HPL phase by redistribution of the blend chains. The diversity of structures observed in the morphology diagram (interfacial energy and blend composition parameter space) highlights that blends are responsive materials, where one can select the morphology using

boundary conditions. We exploit this responsiveness to demonstrate microscale patterning of morphology by casting blend films on top of multi-tone chemical patterns.

Results and Discussion

Conventional single-component BCP films form ordered phases that depend on film thickness and substrate surface energy. Blends of block copolymers are more strongly responsive to local conditions (Fig. 1), which allows them to form coexistence phases.[84, 85] We studied thin film blends of cylinder-forming (C) and lamellar-forming (L) polystyrene-*block*-poly(methyl methacrylate) (PS-*b*-PMMA), and found that the interplay of blending and substrate surface energy can be used to control the morphology that arises. We first consider the assembly of a thin film of pure C67 (cylinder-forming PS-*b*-PMMA with total molecular weight of 67 kg mol^{-1}) as a function of film thickness (Fig. 2). When film thickness is commensurate with a given state (e.g., integer number of layers of horizontally oriented cylinders), that state is preferred. Incommensurate thicknesses generate an energy penalty, which can cause the system to convert into another orientation or even another morphology. For C67 on a slightly MMA-preferential substrate (PS-*r*-PMMA brush with 20% PS content), we observe the appearance of a PMMA honeycomb with PS perforations, which can be assigned to the HPL phase (Fig. 2, 39 nm). In a pure C67 film, the HPL appears only in coexistence with regions of (distorted) horizontal cylinders.

Blending C67 with L75, a lamellar-forming polymer of similar molecular weight (PS-*b*-PMMA, 75 kg mol^{-1}), and casting on a range of substrate energies, yields a wide variety of morphologies (Fig. 3 and Supporting Information, SI, Fig. S1); both pure phases and coexistence phases appear. Morphologies were assigned using scanning electron microscopy (SEM) images

(see SI Figs S2–S4) and grazing-incidence small-angle x-ray scattering (SI Figs S5 and S6). Considering first the endpoints of the blend composition axis, we observe expected morphologies. For pure C67, preferential substrate wetting yields horizontal cylinders (line pattern), whereas vertical cylinders (dot patterns) form at intermediate surface energies (balanced interaction with PS and PMMA blocks). For pure L75, preferential wetting yields horizontal lamellae (which appear featureless) when the thickness is commensurate for the wetting condition, or terraced (islands/holes) when incommensurate. For neutral surface energies, L75 forms vertical lamellae (line patterns).

Blends exhibit several motifs distinct from the pure constituents (Fig. 3, middle rows). In some cases, the blend forms a coexistence of different structures, suggesting that blending has decreased the energy difference between the states. Over a broad range of conditions, the blends form a pure HPL phase (Fig. 3, purple; confirmed using cross-section SEM as shown in SI Fig. S7). This can be contrasted to pure C67, where the HPL appears mixed with other structures. Blends also allow perforations to appear in horizontal lamellae. Taken together, these results suggest that blending has stabilized the HPL phase, making it more easily accessible.[55, 79] The blend materials are responsive along both axes of the morphology diagram. By adjusting blend composition, one can access different suites of phases. By adjusting the substrate surface energy, a particular blend composition can exhibit a variety of distinct phases. For instance, the 50:50 blend can form HPL, line patterns, or horizontal lamellae, depending on the underlying surface energy.

The role of substrate surface energy can be understood in terms of the energy balance for materials to be in contact with the substrate. In pure BCP materials, a preferred orientation is selected based on substrate contact. In general, horizontal morphologies arise for selective

substrates, since one of the components (majority or minority BCP block) will preferentially wet the substrate interface. Vertical morphologies instead arise when the substrate is roughly neutral (equal interaction with both blocks). The additional configurational freedom afforded by blends provides access to a wider range of possible morphologies. Substrate energy can then select among them; in particular selecting the morphology that maximizes favorable contact with the substrate (that is, where the BCP average composition matches the substrate energy). In doing so, the blends have an additional degree-of-freedom (compared to pure materials), since chains can locally redistribute to maximize favorable substrate contacts. For instance, the HPL phase forms on hydrophilic substrates since it involves a uniform wetting layer of the minority (PMMA) block.

In addition to morphology, the blend repeat-spacing (L_0) is also responsive to substrate conditions. For instance, the 50:50 blend HPL phase L_0 varies by ~4%, from 43 nm to 45 nm. The blend HPL L_0 is substantially larger than the HPL formed by pure C67 (38 nm), and larger than the L_0 of either pure component (SI Fig. S4); 34 nm for C67 and 39 nm for L75. This apparent swelling suggests a distinct packing of the underlying chains in the blend HPL phase.

The structures formed by blends may deviate from the corresponding bulk equilibrium morphology. For instance, the morphology diagram exhibits a broad region of line patterns; one can in fact identify a continuous transition from horizontal cylinders to vertical lamellae through the morphology diagram (all appearing as line patterns in top-view SEM images). Structurally, this must correspond to a continuum through rounded lamellae and distorted cylinders. Similarly, several blend HPL morphologies exhibit distorted packing and strut-geometry (e.g. Fig. 3, 25:75 blend on SiO_2 substrate) compared to the canonical HPL. This confirms that blending accommodates distorted morphologies, stabilizing otherwise prohibitively high-energy states.

An important question with blends is whether the underlying chains phase separate during structure formation. The homogeneous phases, including HPL, strongly suggest that chains are mixing to form a single compromise morphology, as would be predicted from entropic arguments (strong driving force for mixing). The coexistence phases (e.g. dots and lines), however, could be interpreted as local demixing of chains into equilibrium morphologies. Experimentally, we find that the L_0 of coexisting regions match each other (and are distorted from the pure material L_0).[84] Coarse-grained molecular dynamics simulations showed that both chain types participate in the formation of coexistence phases,[85] though with small statistical excesses of chain types (e.g. slightly more L chains in lamellar-like line objects) and with rearrangement of chains within morphological objects to stabilize them (e.g. slightly more C chains segregated to the rounded end-caps of line objects). The present results are consistent with these arguments; we interpret the observed morphologies as resulting from mixing of chains, with local redistribution of chains stabilizing otherwise high-energy motifs.

The film thickness (43 nm) selected for the results shown in Figure 3 is slightly thicker than the L_0 of either pure material (34 nm for C67, 39 nm for L75). This roughly monolayer regime provides the opportunity for both horizontal and vertical morphologies to develop (the former are disfavored in ultrathin films, the latter are rare in thicker films), as observed experimentally. It is important to note that BCPs are strongly sensitive to film thickness, since if a given thickness is incommensurate with a particular morphology/orientation, then it will be destabilized. Thus, we expect the observed phases for blends to change if film thickness is modified. We observe that blending affords tolerance to variations in thickness (Fig. 4). The blend forms a pure HPL over a broad thickness range, whereas pure C67 forms coexistence states across the same thickness range. In BCP research, it is often assumed that film thickness trends arise due to the thickness

itself (confinement size scale, ordering at interfaces, etc.). However, one must also recognize that adjusting film thickness via spin-coating introduces an additional consideration, since casting conditions affect solvent evaporation rate, which influences ordering (directional and/or latent ordering).[90-92] This is especially relevant when considering possibly metastable ordering, as we do here. We observe that evaporation rate influences the appearance of HPL (SI Figs S8 and S9). This implies that observed trends as a function of thickness arise both due to intrinsic thickness effects and casting effects. While C67 can form a pure and well-ordered HPL if conditions are tuned precisely, a blend exhibits pure HPL over a much broader range of conditions. This ability of the blend to accommodate local morphological distortions introduces a tradeoff, making it both able to form the HPL phase, and also stabilizing more distortions (e.g. variability in pore size for HPL).

To elucidate the mechanism of blend structure formation, it is illustrative to compare the ordering exhibited in blends having different constituent chains, but the same overall block composition ratio. For example, Figure 5 shows morphologies for 12 different blend films, combining different materials but adjusting concentration to maintain an overall PS:PMMA ratio of 0.6:0.4. The wide variety of exhibited patterns (Fig. 5) demonstrates that the overall block ratio cannot by itself explain the observed phases. For instance, blends of cylinder-forming (C) (PMMA cores in a PS matrix) and inverse-cylinder (O) (PS cores in a PMMA matrix) BCPs form lamellar phases since the intrinsic interfacial curvatures of the constituent chains cancel one another (Fig. 5, bottom row). However, blends of C and L with the same overall PS:PMMA ratio instead form HPL in most cases (Fig. 5, top three rows of blue boxed-in region), since the constituent chains can reorganize to stabilize perforations. This demonstrates that morphology depends on the architecture of the underlying chains, and not simply on the overall volume

fraction of components (PS and PMMA). It is worth noting that the precise phases observed depend in part on film thickness, since the commensurability regime will be different for materials with different L_0. Nevertheless, the underlying trends provide insights into ordering. It is interesting to note that blends of disparate molecular weights (M_w) can form HPL phases or HPL-like defects, regardless of which component provides the longer chains. The size of perforations increases with the M_w of both constituents, implying that both chain types contribute to their formation.

These observations suggest that morphological stabilization occurs due to the underlying propensity for BCP chains to localize so as to reduce energy and stabilize defects (Fig. 6).[18, 19, 85] In a blend, the constituent chains redistribute to accommodate local curvature and reduce the energy of the morphology. For instance, the HPL phase can be thought of as a defective version of a lamellar phase, with perforations introduced into the lamellar sheets. While perforations are high energy in a pure L system, the introduction of cylinder chains stabilizes these defects, because C chains can accommodate the higher curvature of the pore and the C chain's longer majority (PS) chain end fills in the perforation. This explains the isolated perforation defects observed in lamellar phases when C chains are present (Fig. 3, 75:25 blend on 80% PS substrate). Similarly, one can consider some blend morphologies as defective cylinder phases. Cross-connections between cylinders in a pure C system are high-energy and disappear as annealing proceeds. However, introducing L chains stabilizes these defects, accommodating the lower local curvature and providing the larger minority chain-end necessary to fill in the junction point. The result can be the formation of local hole-like motifs in an otherwise horizontal-cylinder morphology (Fig. 3, 25:75 blend on 20% PS substrate). This chain redistribution argument is general, explaining the observed diversity of morphologies and distortions. In each

case, the mixture of chains in a blend provides access to a much broader range of local structural motifs, and a correspondingly broader range of morphologies.

Nanoscale chemical patterning is frequently used to prescribe the positional ordering of PS-*b*-PMMA thin films.[13, 86, 93-97] Here, armed with an understanding of blend responsiveness, we can also employ microscale patterning of surface chemistry to direct *morphology formation*. We developed a workflow to generate multi-tone (2-tone, 3-tone, etc.) chemical patterns through iterative application of PS-*r*-PMMA brush layers, electron-beam lithography (EBL), and plasma etching (Fig. 7 and SI Fig. S10). A blend BCP film is cast on the patterned substrate and thermally annealed, giving rise to multiple morphologies based on the local substrate chemistry. The material response is highly local (on the order of the BCP repeat-spacing) and thus allows the creation of desired nanoscale morphologies, localized in a prescribed manner at the nano/microscale (SI Figs S11-S14). The 3-tone surface pattern shown in Fig. 7 exhibits four distinct structural patterns (dot patterns, line patterns, HPL, horizontal lamellae) organized into three regions, defined by the underlying surface chemistry. This highlights the utility of blends as responsive materials, capable of generating different nanoscale patterns simultaneously and in a positionally-prescribed manner. Because nanostructure dictates a host of bulk properties,[98] including wettability,[12, 99-101] optical response,[102-104] and electrical properties,[16, 105, 106], these results suggest that blends could enable a rich set of new functional coatings.

Conclusion

We explored the ordering of blends of cylinder-forming and lamellar-forming BCP materials as a function of blend composition and substrate surface energy. Blending stabilizes a host of otherwise inaccessible states, including coexistence phases, and a pure HPL phase that is

typically metastable and difficult to form in pure materials. Blending accommodates significant swelling of repeat-spacing, providing access to a broader range of length scales. We ascribe the observed behavior to the enhanced packing freedom available to blends, wherein the constituent chains are able to reorganize locally to stabilize different structural motifs. Blends can stabilize defects and morphologies that would be otherwise inaccessible due to being high-energy or protected by energy barriers.

These results imply that more extreme blending could stabilize yet more exotic morphologies. For instance, the freedom afforded by a three-component blend might stabilize motifs that typically require strong directing fields. However, we also note that the stabilization of defect-states incurs a tradeoff. For instance, blending makes the HPL phase more accessible, but it also makes the resultant morphologies more defective. In the limiting case, extreme blending is equivalent to a highly polydisperse BCP material, which forms highly defective morphologies that may lack a definite repeating structure. Nevertheless, it appears possible to engineer morphologies by blending different BCP chains and directing their ordering using boundary conditions and other external forces.

This work demonstrates that the morphological state and repeat-spacing are responsive to the underlying surface energy. This work is consistent with a growing body of results showing that blends of different BCP chains can yield a greater diversity of local motifs and global morphologies than their constituent materials,[84, 85] and that the precise structure that forms is responsive to boundary conditions (thickness, interfacial energies, substrate chemical patterns)[19, 69, 86, 107] and ordering history.[18] BCPs are also strongly sensitive to annealing conditions, and it would thus be instructive in the future to study ordering of the blends described herein as a function of annealing temperature and time. This would provide evidence regarding which

phases are metastable vs. equilibrium. We exploited this responsiveness to demonstrate microscale patterning of the morphology itself, where four distinct ordering motifs can all coexist in prescribed proximity. This points towards more advanced functional coatings that combine different nanopattern properties to yield materials with a desired emergent response.

Methods

Substrates: 500 μm thick, boron-doped ⟨100⟩ oriented silicon wafers were plasma cleaned for 5 min (March CS-1701) using 100 mTorr O_2, 20 W RF power. Substrates were used either with the bare SiO_2 surface, or after being coated with hydroxy-terminated PS-*r*-PMMA random copolymer brushes having compositions varying from 10–80% PS (provided by The Dow Chemical Company), cast from solution (1.0% wt in propylene glycol methyl ether acetate, PGMEA) via spin-casting (1500 rpm, 45 s). Throughout the manuscript, substrate coating is denoted by the percentage PS content of the coating brush. Substrates with a brush layer were baked on a hotplate under a flow of N_2 gas at 250 °C for 5 min and rinsed in toluene prior to coating with the block copolymer or block copolymer blend film.

Polymer Materials: Block copolymers of PS-*b*-PMMA were used in this work. We define a sample code MXX, where M denotes the morphology (L for lamellar-forming material with approximately equal PS and PMMA volume fractions; C for cylinder-forming material with PMMA as minority; O for inverse cylinder materials with PMMA as matrix) and XX denotes the total molecular weight (M_w) in kg mol^{-1}. The block copolymer materials used in these experiments were purchased from Polymer Source, Inc. and have the following characteristics. Cylindrical phase (C48): M_w = 48 kg/mol, PS:PMMA = 0.7:0.3, PDI = 1.1; (C67): M_w = 67 kg/mol, PS:PMMA = 0.7:0.3, PDI = 1.1; (C99): M_w = 99 kg/mol, PS:PMMA = 0.7:0.3, PDI = 1.1. Lamellar phase (L36): M_w = 36 kg/mol, PS:PMMA = 0.5:0.5, PDI = 1.06; (L75): M_w = 75 kg/mol, PS:PMMA = 0.5:0.5, PDI = 1.1; (L104): M_w = 104 kg/mol, PS:PMMA = 0.5:0.5, PDI = 1.09. Inverse cylinder phase (O71): M_w = 71 kg/mol, PS:PMMA = 0.3:0.7, PDI = 1.06. The repeat-spacing (L_0) of materials was measured by fitting the primary peak position in the Fourier transform of SEM images of homogeneous and well-ordered canonical morphologies (SI Fig. S4). We note that for cylinder-forming materials, the measured L_0 corresponds to the cylinder layering (row-row distance) and so the cylinder-cylinder distance is $d = 2L_0/\sqrt{3}$. For C67, we measured L_0 = 34 nm (d = 39 nm), and for L75 we measured L_0 = 39 nm.

Polymer Films: Block copolymer thin films were applied by spin-casting the neat or blended PS-*b*-PMMA solutions (1% wt. in toluene unless otherwise noted) for 45 s at a rotation speed (between 1200–3600 rpm) selected to yield different film thicknesses. The film thicknesses

studied in this work span a range of thicknesses between 32 nm and 65 nm. We focus studies on films of thickness 43 nm, which is roughly the monolayer regime (slightly thicker than L_0 for either pure material), which affords the possibility for both vertical and horizontal morphologies to develop. The blends were made by combining solid C and L forming PS-*b*-PMMA in either 100:0, 75:25, 50:50, 25:75, or 0:100 ratios by weight. C and O forming PS-*b*-PMMA blends were made in a 1:1.6 ratio to maintain an overall PS fraction of 60 %. Block copolymer films were annealed on a hotplate under a flow of N_2 gas at 250 °C for 5 min.

Material Conversion: To improve contrast for SEM imaging and create inorganic replicas of the nanostructured films, the PMMA domains were converted into aluminum oxide replicas using sequential infiltration synthesis (SIS)[108, 109] using our previously-published protocol.[16, 17] Samples were exposed to four sequential cycles of trimethylaluminum followed by water vapor using a Cambridge Nanotech atomic layer deposition (ALD) tool (100 s exposure at 85 °C). The PS domains were then removed using oxygen plasma etching for 5 min.

Chemical Patterning of Silicon Substrates: Chemical guide patterns were fabricated using electron beam lithography (EBL). Initially, Ti/Au alignment markers were fabricated on silicon substrates by using a standard lift-off technique with optical lithography. Cleaned substrates were treated with an 60% PS brush as previously described. Subsequently, PMMA A2 (MicroChem Inc.) resist was spin-coated onto the substrate (5000 rpm for 60 s) followed by baking on a hotplate at 180 °C for 3 min. The desired regions were then exposed in a JEOL JBX6300-FS electron beam lithography tool using 1 nA beam current at 1250 $\mu C\ cm^{-2}$ using the prefabricated alignment markers as reference. Samples were then developed in a methyl isobutyl ketone: isopropyl alcohol (IPA)(1:3) solution at room temperature for 60 s and rinsed in IPA for 15 s followed by blow drying with N_2 gun. Exposed pattern regions revealed the 60% PS brush underneath, which was then removed by oxygen plasma for 15 s (revealing the underlying SiO_2 surface). The remaining PMMA resist was then stripped off by sonication in toluene (room temperature for 90 s). Subsequently, a 10% PS brush (which selectively binds to the exposed SiO_2 regions) was coated onto the substrate surface and baked, thus creating 2-tone patterned substrates, with exposed regions being more hydrophilic (10% PS brush). The EBL process was then repeated to desired regions using the same alignment markers as the first EBL step and SiO_2 was revealed in these areas. A 80% PS brush was then coated and baked to achieve a 3-tone patterned substrate. Finally, the 50:50 BCP blend was spin casted on the 3-tone patterned substrate followed by self-assembly as previously described.

Imaging and Image Analysis: Samples (inorganic replicas of the BCP structure) were imaged using SEM (Hitachi S-4800) both top-down and at a 70° tilt angle. Custom Python software was used to analyze images.[30, 110] Morphological repeat-spacing was extracted from SEM images by computing the fast Fourier transform (FFT), fitting a Gaussian function to the primary peak position, and converting from this inverse-space position (q) into repeat-spacing (L_0) using $L_0 = 2\pi/q$.

GISAXS: Grazing-incidence small-angle x-ray scattering (GISAXS) measurements were performed at the Complex Materials Scattering (CMS, 11-BM) beamline at the National Synchrotron Light Source II (NSLS-II). Samples were measured at 25 °C in vacuum using an x-ray beam set to an energy of 13.5 keV (wavelength 0.0918 nm) and a beam size of 50 μm tall by

200 μm wide. Two-dimensional scattering images were collected using a photon-counting area detector (Dectris Pilatus, pixel size 172 μm) positioned ~5 m downstream of the sample.

Figures

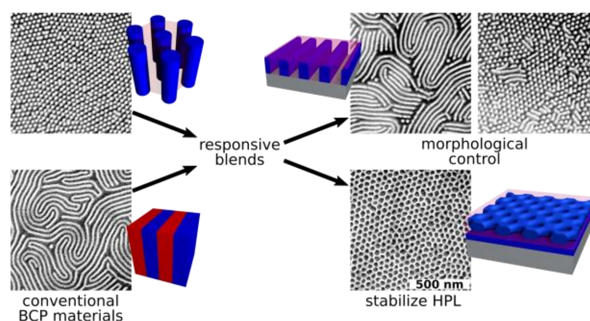

Figure 1: BCP thin films conventionally form a single morphology (such as cylinders or lamellae), dictated by the chain architecture. Blends of BCP materials are responsive, with the morphology that arises depending on external constraints, such as film thickness and substrate surface energy. Such responsive blends can be thought of as a single material whose nanostructure can be tuned by local conditions, allowing the selection of a particular morphology. Moreover, the mixture of underlying chains can stabilize morphologies that are metastable in pure materials, allowing the more facile creation of the HPL phase.

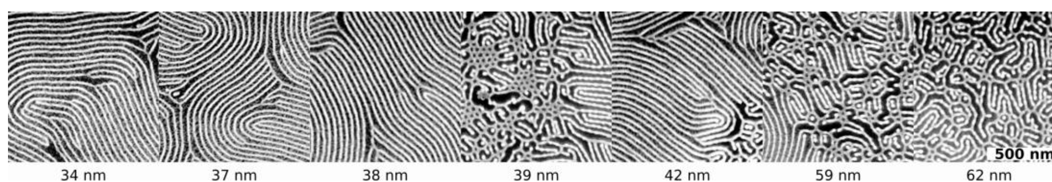

Figure 2: Morphology formation for pure C67 (cylinder-forming PS-*b*-PMMA, 67 kg mol^{-1}) as a function of film thickness (noted below each image). SEM images are captured on inorganic replica films; the converted PMMA regions appear bright in the images while the dark regions correspond to the removed PS matrix. Film thickness was controlled by spin-coating rotation speed, cast on 20% PS substrates (PS-*r*-PMMA brush with 20:80 ratio), and annealed for 5 minutes at 248 °C. The morphology that arises depends strongly on film thickness. For certain thickness ranges, a coexistence of morphologies or orientations is observed. Over a narrow thickness range, the HPL phase coexists with in-plane (horizontal orientation) cylinders. The scale bar (500 nm) applies to all images.

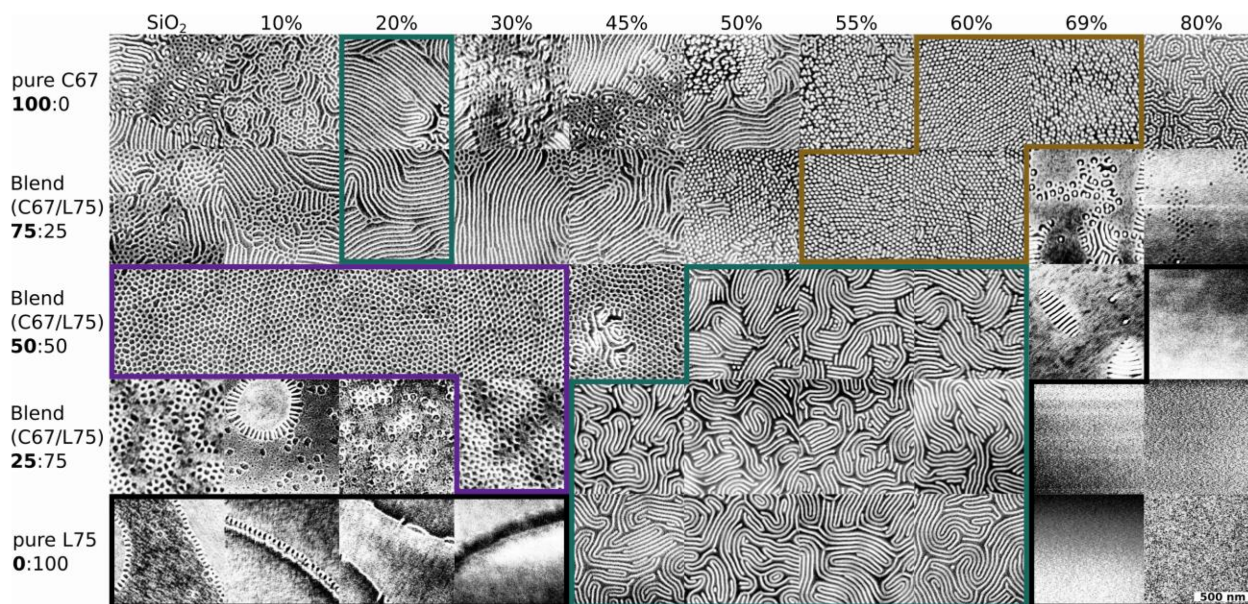

Figure 3: Morphology diagram (SEM images) for BCP pure and blend thin films (43 nm thickness) on a range of substrate surface energies, after thermal annealing (248 °C for 5 min). The rows correspond to different blend ratios of C67 and L75. The columns correspond to different substrate conditions, from SiO_2 (highly hydrophilic, preferential for the PMMA minority block) to 80% PS brush (hydrophobic and preferential for the PS majority block). A range of different pure and coexisting morphologies are observed, including line-patterns (**teal** outline; horizontal cylinders or vertical lamellae), dot-patterns (**gold** outline; vertical cylinders), and flat films (**black** outline; horizontal lamellae). Of note is a large region where a pure HPL phase appears (**purple** outline). The scale bar (500 nm) applies to all images.

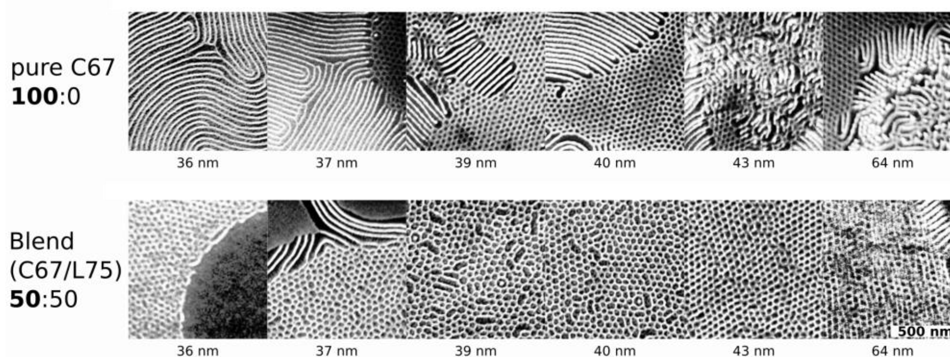

Figure 4: Blending enables more robust formation of the HPL phase. Representative images for pure C67 (top row) and a blend of C67 and L75 (bottom row) are shown for a range of thicknesses (noted below each image), cast on 30% PS substrates. While pure C67 demonstrates coexistence of HPL in some cases, the blend shows a homogeneous HPL phase over a wide thickness range. The scale bar (500 nm) applies to all images.

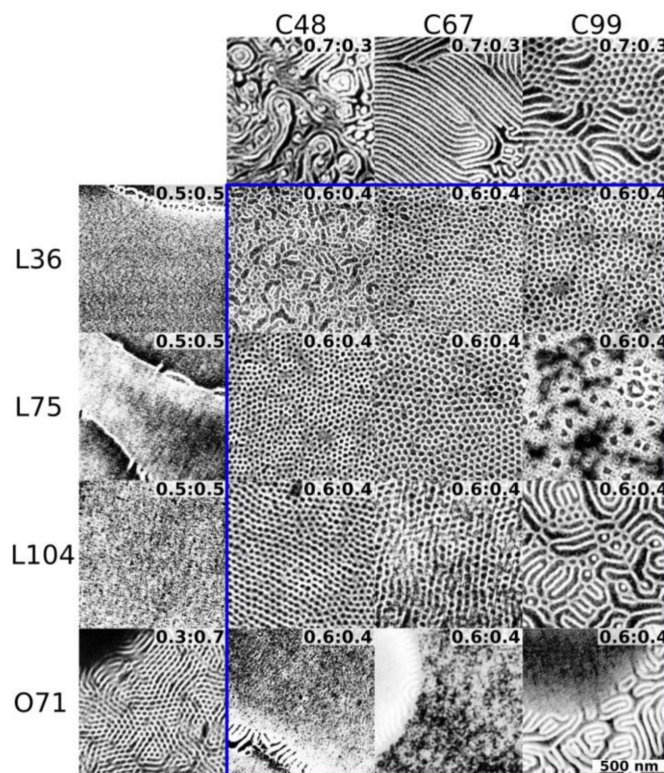

Figure 5: Morphologies for a range of blend materials with identical overall composition ratio (43 nm films on substrate 20% PS brush). The pure materials (C for cylinder-forming, L for lamellar-forming, and O for inverse cylinder-forming; digits denote molecular weight) are shown across the top row and leftmost column; the corresponding blends of all combinations are shown within the blue rectangle. In terms of the PS:PMMA ratios, the C materials are 0.7:0.3, L are 0.5:0.5, and O is 0.3:0.7. The C/L blends are 1:1 by mass, giving rise to an overall PS:PMMA composition of 0.6:0.4. The C/O blends are prepared as 1:1.6 by mass in order to achieve the same overall composition of 0.6:0.4. The C/O blends form distinctly different morphologies from the C/L blends, emphasizing that stabilization of the HPL phase occurs through redistribution of the underlying BCP chains, and is not merely a result of the average interfacial curvature.

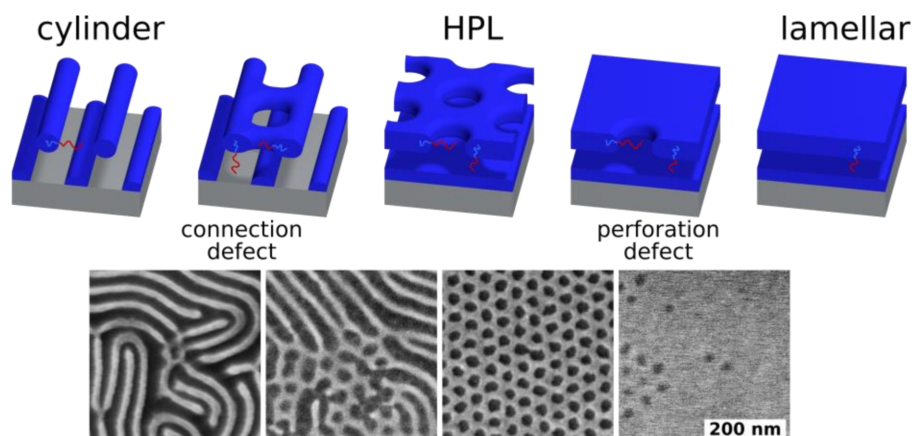

Figure 6: BCP chains localize to stabilize defects. One can conceive a continuous transformation from horizontal cylinders to HPL to horizontal lamellae (top). The intermediate state between cylinder and HPL exhibits connections between adjacent cylinders which form a local hole. This defect is high-energy in a canonical cylinder phase. Yet the introduction of lamellar chains stabilizes the defect since these can accommodate the lower interfacial curvature and swollen minority domains. Similarly, the intermediate state between HPL and lamellae can be thought of as a lamellar sheet with isolated perforation defects. These defects can be stabilized by localizing cylinder chains, which accommodate the higher interfacial curvature and provide the larger majority chain-end content required to construct the pore (which is a connection between adjacent majority/matrix layers). These defective intermediate states are observed experimentally (bottom).

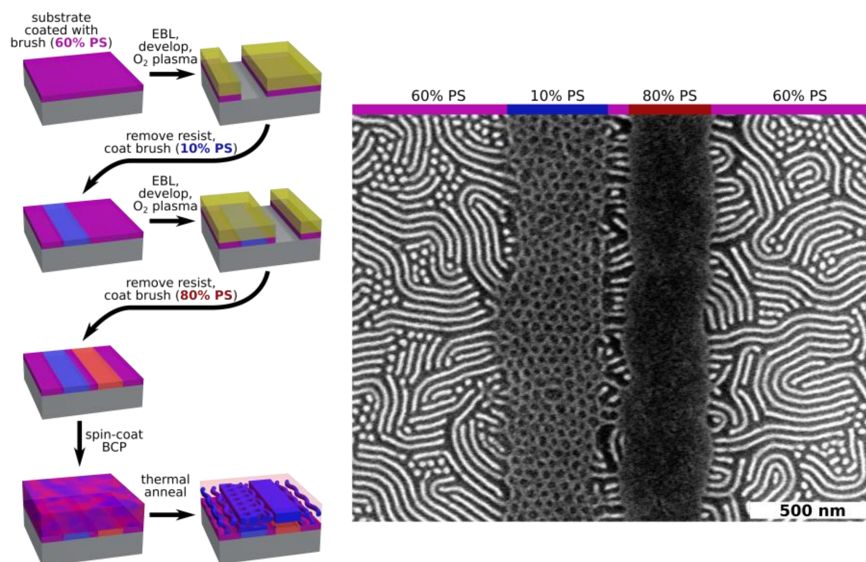

Figure 7: Multi-tone chemical patterns can be used to locally select the BCP morphology of a responsive blend (50:50 blend of C67 and L75). Electron beam lithography is used to define the chemical patterns (left), by exposing and etching to the underlying SiO_2 surface, making it available for the attachment of another brush. By iterating, a substrate exhibiting 3-tone chemistry (3 different brushes in different regions) is fabricated. When a BCP blend orders on such a substrate, the local morphology is selected by the underlying chemistry (right), allowing micro-patterning of the BCP morphology. In the presented example, hydrophilic regions (10% PS brush) generate an HPL morphology, hydrophobic regions (80% PS brush) generate horizontal lamellae, and neutral regions (60% brush) generate a coexistence of lines and dots. Thus, four distinct structural patterns, organized into three distinct regions, are represented.

Supporting Information

Supporting Information provides Fourier analysis of SEM images, x-ray scattering confirmation of morphologies, evidence of thickness and evaporation-rate effects, detailed patterning workflow, and examples and BCP ordering on multi-tone chemical patterns.

Acknowledgements

This research was performed by the Center for Functional Nanomaterials, and used resources of the National Synchrotron Lights Source II, which are U.S. DOE Office of Science Facilities, at Brookhaven National Laboratory under Contract No. DE-SC0012704.

References

1. Bates, F. S.; Fredrickson, G. H., Block Copolymers—Designer Soft Materials. *Physics Today* **1999**, 32.
2. Doerk, G. S.; Yager, K. G., Beyond native block copolymer morphologies. *Molecular Systems Design & Engineering* **2017,** *2* (5), 518-538.
3. Fasolka, M. J.; Mayes, A. M., Block Copolymer Thin Films: Physics and Applications. *Annu. Rev. Mater. Res.* **2001,** *31* (1), 323-355.
4. Albert, J. N. L.; Epps, T. H., Self-assembly of block copolymer thin films. *Mater. today* **2010,** *13* (6), 24-33.
5. Hawker, C. J.; Russell, T. P., Block copolymer lithography: Merging "bottom-up" with "top-down" processes. *Mrs Bull* **2005,** *30* (12), 952-966.
6. Kim, D. H.; Lau, K. H. A.; Robertson, J. W. F.; Lee, O.-J.; Jeong, U.; Lee, J. I.; Hawker, C. J.; Russell, T. P.; Kim, J. K.; Knoll, W., Thin Films of Block Copolymers as Planar Optical Waveguides. *Adv. Mater.* **2005,** *17* (20), 2442-2446.
7. Mecke, A.; Dittrich, C.; Meier, W., Biomimetic membranes designed from amphiphilic block copolymers. *Soft Matter* **2006,** *2* (9), 751-759.
8. Black, C. T.; Ruiz, R.; Breyta, G.; Cheng, J. Y.; Colburn, M. E.; Guarini, K. W.; Kim, H.-C.; Zhang, Y., Polymer self assembly in semiconductor microelectronics. *IBM Journal of Research and Development* **2007,** *51* (5), 605.
9. Darling, S. B., Directing the self-assembly of block copolymers. *Prog. Polym. Sci.* **2007,** *32* (10), 1152-1204.
10. Hamley, I. W., Ordering in thin films of block copolymers: Fundamentals to potential applications. *Prog. Polym. Sci.* **2009,** *34* (11), 1161-1210.
11. Topham, P. D.; Parnell, A. J.; Hiorns, R. C., Block copolymer strategies for solar cell technology. *J. Polym. Sci., Part B: Polym. Phys.* **2011,** *49* (16), 1131-1156.
12. Checco, A.; Rahman, A.; Black, C. T., Robust Superhydrophobicity in Large-Area Nanostructured Surfaces Defined by Block-Copolymer Self Assembly. *Adv. Mater.* **2014,** *26* (6), 886-891.

13. Liu, G.; Detcheverry, F.; Ramírez-Hernández, A.; Yoshida, H.; Tada, Y.; de Pablo, J. J.; Nealey, P. F., Nonbulk Complex Structures in Thin Films of Symmetric Block Copolymers on Chemically Nanopatterned Surfaces. *Macromol.* **2012,** *45* (9), 3986-3992.
14. Tavakkoli K. G, A.; Nicaise, S. M.; Hannon, A. F.; Gotrik, K. W.; Alexander-Katz, A.; Ross, C. A.; Berggren, K. K., Sacrificial-Post Templating Method for Block Copolymer Self-Assembly. *Small* **2014,** *10* (3), 493-499.
15. Chang, J.-B.; Choi, H. K.; Hannon, A. F.; Alexander-Katz, A.; Ross, C. A.; Berggren, K. K., Design rules for self-assembled block copolymer patterns using tiled templates. *Nat Commun* **2014,** *5*, 3305.
16. Majewski, P. W.; Rahman, A.; Black, C. T.; Yager, K. G., Arbitrary lattice symmetries via block copolymer nanomeshes. *Nat. Commun.* **2015,** *6*, 7448.
17. Rahman, A.; Majewski, P. W.; Doerk, G.; Black, C. T.; Yager, K. G., Non-native three-dimensional block copolymer morphologies. *Nat. Commun.* **2016,** *7*, 13988.
18. Russell, S. T.; Bae, S.; Subramanian, A.; Tiwale, N.; Doerk, G.; Nam, C.-Y.; Fukuto, M.; Yager, K. G., Priming self-assembly pathways by stacking block copolymers. *Nat. Commun.* **2022,** *13* (1), 6947.
19. Doerk, G. S.; Stein, A.; Bae, S.; Noack, M. M.; Fukuto, M.; Yager, K. G., Autonomous discovery of emergent morphologies in directed self-assembly of block copolymer blends. *Science Advances* **2023,** *9* (2), eadd3687.
20. Leibler, L., Theory of Microphase Separation in Block Copolymers. *Macromol.* **1980,** *13* (6), 1602-1617.
21. Bates, F. S.; Fredrickson, G. H., Block Copolymer Thermodynamics: Theory and Experiment. *Annu. Rev. Phys. Chem.* **1990,** *41* (1), 525-557.
22. Bates, F. S.; Schulz, M. F.; Khandpur, A. K.; Forster, S.; Rosedale, J. H.; Almdal, K.; Mortensen, K., Fluctuations, conformational asymmetry and block copolymer phase behaviour. *Faraday Discuss.* **1994,** *98* (0), 7-18.
23. Hajduk, D. A.; Takenouchi, H.; Hillmyer, M. A.; Bates, F. S.; Vigild, M. E.; Almdal, K., Stability of the Perforated Layer (PL) Phase in Diblock Copolymer Melts. *Macromol.* **1997,** *30* (13), 3788-3795.
24. Beardsley, T. M.; Matsen, M. W., Monte Carlo phase diagram for diblock copolymer melts. *The European Physical Journal E* **2010,** *32* (3), 255-264.
25. Sun, Z.; Liu, R.; Su, T.; Huang, H.; Kawamoto, K.; Liang, R.; Liu, B.; Zhong, M.; Alexander-Katz, A.; Ross, C. A.; Johnson, J. A., Emergence of layered nanoscale mesh networks through intrinsic molecular confinement self-assembly. *Nat. Nanotechnol.* **2023**.
26. Koo, K.; Ahn, H.; Kim, S.-W.; Ryu, D. Y.; Russell, T. P., Directed self-assembly of block copolymers in the extreme: guiding microdomains from the small to the large. *Soft Matter* **2013,** *9* (38), 9059-9071.
27. Luo, M.; Epps, T. H., Directed Block Copolymer Thin Film Self-Assembly: Emerging Trends in Nanopattern Fabrication. *Macromol.* **2013,** *46* (19), 7567-7579.
28. Hu, H.; Gopinadhan, M.; Osuji, C. O., Directed self-assembly of block copolymers: a tutorial review of strategies for enabling nanotechnology with soft matter. *Soft Matter* **2014,** *10* (22), 3867-3889.
29. Majewski, P. W.; Yager, K. G., Rapid ordering of block copolymer thin films. *Journal of Physics: Condensed Matter* **2016,** *28* (40), 403002.
30. Majewski, P. W.; Yager, K. G., Reordering transitions during annealing of block copolymer cylinder phases. *Soft Matter* **2016,** *12*, 281-294.

31. Choo, Y.; Majewski, P. W.; Fukuto, M.; Osuji, C. O.; Yager, K. G., Pathway-engineering for highly-aligned block copolymer arrays. *Nanoscale* **2018,** *10* (1), 416-427.
32. Albert, J. N. L.; Bogart, T. D.; Lewis, R. L.; Beers, K. L.; Fasolka, M. J.; Hutchison, J. B.; Vogt, B. D.; Epps, T. H., Gradient Solvent Vapor Annealing of Block Copolymer Thin Films Using a Microfluidic Mixing Device. *Nano Lett.* **2011,** *11* (3), 1351-1357.
33. Hannon, A. F.; Bai, W.; Alexander-Katz, A.; Ross, C. A., Simulation methods for solvent vapor annealing of block copolymer thin films. *Soft Matter* **2015,** *11* (19), 3794-3805.
34. Mansky, P.; Russell, T. P.; Hawker, C. J.; Mays, J.; Cook, D. C.; Satija, S. K., Interfacial Segregation in Disordered Block Copolymers: Effect of Tunable Surface Potentials. *Phys. Rev. Lett.* **1997,** *79* (2), 237.
35. Huang, E.; Rockford, L.; Russell, T. P.; Hawker, C. J., Nanodomain control in copolymer thin films. *Nature* **1998,** *395* (6704), 757.
36. Han, E.; Stuen, K. O.; Leolukman, M.; Liu, C.-C.; Nealey, P. F.; Gopalan, P., Perpendicular Orientation of Domains in Cylinder-Forming Block Copolymer Thick Films by Controlled Interfacial Interactions. *Macromol.* **2009,** *42* (13), 4896-4901.
37. Kim, H.-C.; Rettner, C. T.; Sundstr, L., Fabrication of 20nm half-pitch gratings by corrugation-directed self-assembly. *Nanotechnology* **2008,** *19* (23), 235301.
38. Park, S.; Lee, D. H.; Xu, J.; Kim, B.; Hong, S. W.; Jeong, U.; Xu, T.; Russell, T. P., Macroscopic 10-Terabit-per-Square-Inch Arrays from Block Copolymers with Lateral Order. *Science* **2009,** *323* (5917), 1030-1033.
39. Yang, X. M.; Peters, R. D.; Nealey, P. F.; Solak, H. H.; Cerrina, F., Guided Self-Assembly of Symmetric Diblock Copolymer Films on Chemically Nanopatterned Substrates. *Macromol.* **2000,** *33* (26), 9575-9582.
40. Kim, S. O.; Solak, H. H.; Stoykovich, M. P.; Ferrier, N. J.; de Pablo, J. J.; Nealey, P. F., Epitaxial self-assembly of block copolymers on lithographically defined nanopatterned substrates. *Nature* **2003,** *424* (6947), 411-414.
41. Koppi, K. A.; Tirrell, M.; Bates, F. S., Shear-induced isotropic-to-lamellar transition. *Phys. Rev. Lett.* **1993,** *70* (10), 1449.
42. Riise, B. L.; Fredrickson, G. H.; Larson, R. G.; Pearson, D. S., Rheology and Shear-Induced Alignment of Lamellar Diblock and Triblock Copolymers. *Macromol.* **1995,** *28* (23), 7653-7659.
43. Angelescu, D. E.; Waller, J. H.; Adamson, D. H.; Deshpande, P.; Chou, S. Y.; Register, R. A.; Chaikin, P. M., Macroscopic Orientation of Block Copolymer Cylinders in Single-Layer Films by Shearing. *Adv. Mater.* **2004,** *16* (19), 1736-1740.
44. Davis, R. L.; Chaikin, P. M.; Register, R. A., Cylinder Orientation and Shear Alignment in Thin Films of Polystyrene–Poly(n-hexyl methacrylate) Diblock Copolymers. *Macromol.* **2014,** *47* (15), 5277-5285.
45. Majewski, P. W.; Yager, K. G., Block Copolymer Response to Photothermal Stress Fields. *Macromol.* **2015,** *48* (13), 4591-4598.
46. Ferrarese Lupi, F.; Giammaria, T. J.; Ceresoli, M.; Seguini, G.; Sparnacci, K.; Antonioli, D.; Gianotti, V.; Laus, M.; Perego, M., Rapid thermal processing of self-assembling block copolymer thin films. *Nanotechnology* **2013,** *24* (31), 315601.
47. Majewski, P. W.; Yager, K. G., Millisecond Ordering of Block Copolymer Films via Photothermal Gradients. *ACS Nano* **2015,** *9* (4), 3896-3906.
48. Nowak, S. R.; Yager, K. G., Photothermally Directed Assembly of Block Copolymers. *Advanced Materials Interfaces* **2020,** *7* (5), 1901679.

49. Hashimoto, T.; Koizumi, S.; Hasegawa, H.; Izumitani, T.; Hyde, S. T., Observation of "mesh" and "strut" structures in block copolymer/homopolymer mixtures. *Macromol.* **1992,** *25* (5), 1433-1439.
50. Almdal, K.; Koppi, K. A.; Bates, F. S.; Mortensen, K., Multiple ordered phases in a block copolymer melt. *Macromol.* **1992,** *25* (6), 1743-1751.
51. Spontak, R. J.; Smith, S. D.; Ashraf, A., Dependence of the OBDD morphology on diblock copolymer molecular weight in copolymer/homopolymer blends. *Macromol.* **1993,** *26* (5), 956-962.
52. Disko, M. M.; Liang, K. S.; Behal, S. K.; Roe, R. J.; Jeon, K. J., Catenoid-lamellar phase in blends of styrene-butadiene diblock copolymer and homopolymer. *Macromol.* **1993,** *26* (11), 2983-2986.
53. Hamley, I. W.; Koppi, K. A.; Rosedale, J. H.; Bates, F. S.; Almdal, K.; Mortensen, K., Hexagonal mesophases between lamellae and cylinders in a diblock copolymer melt. *Macromol.* **1993,** *26* (22), 5959-5970.
54. Foerster, S.; Khandpur, A. K.; Zhao, J.; Bates, F. S.; Hamley, I. W.; Ryan, A. J.; Bras, W., Complex Phase Behavior of Polyisoprene-Polystyrene Diblock Copolymers Near the Order-Disorder Transition. *Macromol.* **1994,** *27* (23), 6922-6935.
55. Loo, Y.-L.; Register, R. A.; Adamson, D. H.; Ryan, A. J., A Highly Regular Hexagonally Perforated Lamellar Structure in a Quiescent Diblock Copolymer. *Macromol.* **2005,** *38* (11), 4947-4949.
56. Ly, D. Q.; Honda, T.; Kawakatsu, T.; Zvelindovsky, A. V., Hexagonally Perforated Lamella-to-Cylinder Transition in a Diblock Copolymer Thin Film under an Electric Field. *Macromol.* **2008,** *41* (12), 4501-4505.
57. Knoll, A.; Magerle, R.; Krausch, G., Phase behavior in thin films of cylinder-forming ABA block copolymers: Experiments. *J. Chem. Phys.* **2004,** *120* (2), 1105-1116.
58. Li, Y.; Huang, H.; He, T.; Gong, Y., Solvent vapor induced morphology transition in thin film of cylinder forming diblock copolymer. *Applied Surface Science* **2011,** *257* (18), 8093-8101.
59. Jung, Y. S.; Ross, C. A., Solvent-Vapor-Induced Tunability of Self-Assembled Block Copolymer Patterns. *Adv. Mater.* **2009,** *21* (24), 2540-2545.
60. Knoll, A.; Horvat, A.; Lyakhova, K. S.; Krausch, G.; Sevink, G. J. A.; Zvelindovsky, A. V.; Magerle, R., Phase Behavior in Thin Films of Cylinder-Forming Block Copolymers. *Phys. Rev. Lett.* **2002,** *89* (3), 035501.
61. Luo, M.; Seppala, J. E.; Albert, J. N. L.; Lewis, R. L.; Mahadevapuram, N.; Stein, G. E.; Epps, T. H., Manipulating Nanoscale Morphologies in Cylinder-Forming Poly(styrene-b-isoprene-b-styrene) Thin Films Using Film Thickness and Substrate Surface Chemistry Gradients. *Macromol.* **2013,** *46* (5), 1803-1811.
62. Park, I.; Park, S.; Park, H.-W.; Chang, T.; Yang, H.; Ryu, C. Y., Unexpected Hexagonally Perforated Layer Morphology of PS-b-PMMA Block Copolymer in Supported Thin Film. *Macromol.* **2006,** *39* (1), 315-318.
63. Tsarkova, L., Distortion of a Unit Cell versus Phase Transition to Nonbulk Morphology in Frustrated Films of Cylinder-Forming Polystyrene-b-polybutadiene Diblock Copolymers. *Macromol.* **2012,** *45* (19), 7985-7994.
64. Doerk, G. S.; Yager, K. G., Rapid Ordering in "Wet Brush" Block Copolymer/Homopolymer Ternary Blends. *ACS Nano* **2017,** *11* (12), 12326-12336.

65. Doerk, G. S.; Li, R.; Fukuto, M.; Yager, K. G., Wet Brush Homopolymers as "Smart Solvents" for Rapid, Large Period Block Copolymer Thin Film Self-Assembly. *Macromol.* **2020,** *53* (3), 1098-1113.
66. Orso, K. A.; Green, P. F., Phase Behavior of Thin Film Blends of Block Copolymers and Homopolymers: Changes in Domain Dimensions. *Macromol.* **1999,** *32* (4), 1087-1092.
67. Peng, J.; Gao, X.; Wei, Y.; Wang, H.; Li, B.; Han, Y., Controlling the size of nanostructures in thin films via blending of block copolymers and homopolymers. *J. Chem. Phys.* **2005,** *122* (11), 114706.
68. Jeong, U.; Ryu, D. Y.; Kho, D. H.; Lee, D. H.; Kim, J. K.; Russell, T. P., Phase Behavior of Mixtures of Block Copolymer and Homopolymers in Thin Films and Bulk. *Macromol.* **2003,** *36* (10), 3626-3634.
69. Toth, K.; Osuji, C. O.; Yager, K. G.; Doerk, G. S., High-throughput morphology mapping of self-assembling ternary polymer blends. *RSC Advances* **2020,** *10* (69), 42529-42541.
70. Hashimoto, T.; Koizumi, S.; Hasegawa, H., Ordered Structure in Blends of Block Copolymers.2.Self-Assembly for Immiscible Lamella-Forming Copolymers. *Macromol.* **1994,** *27* (6), 1562-1570.
71. Koizumi, S.; Hasegawa, H.; Hashimoto, T., Ordered Structure in Blends of Block Copolymers. 3. Self-Assembly in Blends of Sphere- or Cylinder-Forming Copolymers. *Macromol.* **1994,** *27* (15), 4371-4381.
72. Matsen, M. W., Immiscibility of large and small symmetric diblock copolymers. *J. Chem. Phys.* **1995,** *103* (8), 3268-3271.
73. Lipic, P. M.; Bates, F. S.; Matsen, M. W., Non-equilibrium phase behavior of diblock copolymer melts and binary blends in the intermediate segregation regime. *J. Polym. Sci., Part B: Polym. Phys.* **1999,** *37* (16), 2229-2238.
74. Hadziioannou, G.; Skoulios, A., Structural study of mixtures of styrene isoprene two- and three-block copolymers. *Macromol.* **1982,** *15* (2), 267-271.
75. Yamaguchi, D.; Takenaka, M.; Hasegawa, H.; Hashimoto, T., Macro- and Microphase Transitions in Binary Blends of Block Copolymers with Complementarily Asymmetric Compositions. *Macromol.* **2001,** *34* (6), 1707-1719.
76. Court, F.; Hashimoto, T., Morphological Studies of Binary Mixtures of Block Copolymers. 1. Cosurfactant Effects and Composition Dependence of Morphology. *Macromol.* **2001,** *34* (8), 2536-2545.
77. Park, S.-B.; Ha, J.-g.; Hahn, S. K.; Zin, W.-C., Temperature-dependent location of a weakly segregated block copolymer in binary blends of block copolymers. *J. Polym. Sci., Part B: Polym. Phys.* **2014,** *52* (6), 470-476.
78. Rokhlenko, Y.; Majewski, P. W.; Larson, S. R.; Gopalan, P.; Yager, K. G.; Osuji, C. O., Implications of Grain Size Variation in Magnetic Field Alignment of Block Copolymer Blends. *ACS Macro Letters* **2017,** *6* (4), 404-409.
79. Zhao, J.; Majumdar, B.; Schulz, M. F.; Bates, F. S.; Almdal, K.; Mortensen, K.; Hajduk, D. A.; Gruner, S. M., Phase Behavior of Pure Diblocks and Binary Diblock Blends of Poly(ethylene)−Poly(ethylethylene). *Macromol.* **1996,** *29* (4), 1204-1215.
80. Abetz, V.; Goldacker, T., Formation of superlattices via blending of block copolymers. *Macromol. Rapid Commun.* **2000,** *21* (1), 16-34.
81. Spontak, R. J.; Fung, J. C.; Braunfeld, M. B.; Sedat, J. W.; Agard, D. A.; Kane, L.; Smith, S. D.; Satkowski, M. M.; Ashraf, A.; Hajduk, D. A.; Gruner, S. M., Phase Behavior of

Ordered Diblock Copolymer Blends: Effect of Compositional Heterogeneity. *Macromol.* **1996,** *29* (13), 4494-4507.
82. Matsen, M. W.; Bates, F. S., One-Component Approximation for Binary Diblock Copolymer Blends. *Macromol.* **1995,** *28* (21), 7298-7300.
83. Choi, C.; Ahn, S.; Kim, J. K., Diverse Morphologies of Block Copolymers by Blending with Homo (and Co) Polymers. *Macromol.* **2020,** *53* (12), 4577-4580.
84. Yager, K. G.; Lai, E.; Black, C. T., Self-Assembled Phases of Block Copolymer Blend Thin Films. *ACS Nano* **2014,** *8* (10), 10582-10588.
85. Bae, S.; Yager, K. G., Chain Redistribution Stabilizes Coexistence Phases in Block Copolymer Blends. *ACS Nano* **2022,** *16* (10), 17107-17115.
86. Stein, A.; Wright, G.; Yager, K. G.; Doerk, G. S.; Black, C. T., Selective directed self-assembly of coexisting morphologies using block copolymer blends. *Nat. Commun.* **2016,** *7*, 12366.
87. Ham, S.; Shin, C.; Kim, E.; Ryu, D. Y.; Jeong, U.; Russell, T. P.; Hawker, C. J., Microdomain Orientation of PS-b-PMMA by Controlled Interfacial Interactions. *Macromol.* **2008,** *41* (17), 6431-6437.
88. Ryu, D. Y.; Ham, S.; Kim, E.; Jeong, U.; Hawker, C. J.; Russell, T. P., Cylindrical Microdomain Orientation of PS-b-PMMA on the Balanced Interfacial Interactions: Composition Effect of Block Copolymers. *Macromol.* **2009,** *42* (13), 4902-4906.
89. Andreozzi, A.; Poliani, E.; Seguini, G.; Perego, M., The effect of random copolymer on the characteristic dimensions of cylinder-forming PS-b-PMMA thin films. *Nanotechnology* **2011,** *22* (18), 185304.
90. Zhang, X.; Yager, K. G.; Kang, S.; Fredin, N. J.; Akgun, B.; Satija, S.; Douglas, J. F.; Karim, A.; Jones, R. L., Solvent Retention in Thin Spin-Coated Polystyrene and Poly(methyl methacrylate) Homopolymer Films Studied By Neutron Reflectometry. *Macromol.* **2009,** *43* (2), 1117-1123.
91. Ebbens, S.; Hodgkinson, R.; Parnell, A. J.; Dunbar, A.; Martin, S. J.; Topham, P. D.; Clarke, N.; Howse, J. R., InSitu Imaging and Height Reconstruction of Phase Separation Processes in Polymer Blends during Spin Coating. *ACS Nano* **2011,** *5* (6), 5124-5131.
92. Zhang, X.; Douglas, J. F.; Jones, R. L., Influence of film casting method on block copolymer ordering in thin films. *Soft Matter* **2012,** *8* (18), 4980-4987.
93. Li, H.-W.; Huck, W. T. S., Ordered Block-Copolymer Assembly Using Nanoimprint Lithography. *Nano Lett.* **2004,** *4* (9), 1633-1636.
94. Edwards, E. W.; Müller, M.; Stoykovich, M. P.; Solak, H. H.; de Pablo, J. J.; Nealey, P. F., Dimensions and Shapes of Block Copolymer Domains Assembled on Lithographically Defined Chemically Patterned Substrates. *Macromol.* **2007,** *40* (1), 90-96.
95. Park, S.-M.; Craig, G. S. W.; La, Y.-H.; Solak, H. H.; Nealey, P. F., Square Arrays of Vertical Cylinders of PS-b-PMMA on Chemically Nanopatterned Surfaces. *Macromol.* **2007,** *40* (14), 5084-5094.
96. Tada, Y.; Akasaka, S.; Yoshida, H.; Hasegawa, H.; Dobisz, E.; Kercher, D.; Takenaka, M., Directed Self-Assembly of Diblock Copolymer Thin Films on Chemically-Patterned Substrates for Defect-Free Nano-Patterning. *Macromol.* **2008,** *41* (23), 9267-9276.
97. Ruiz, R.; Kang, H.; Detcheverry, F. A.; Dobisz, E.; Kercher, D. S.; Albrecht, T. R.; de Pablo, J. J.; Nealey, P. F., Density Multiplication and Improved Lithography by Directed Block Copolymer Assembly. *Science* **2008,** *321* (5891), 936-939.

98. Bai, W.; Ross, C. A., Functional nanostructured materials based on self-assembly of block copolymers. *Mrs Bull* **2016,** *41* (02), 100-107.
99. Checco, A.; Ocko, B. M.; Rahman, A.; Black, C. T.; Tasinkevych, M.; Giacomello, A.; Dietrich, S., Collapse and Reversibility of the Superhydrophobic State on Nanotextured Surfaces. *Phys. Rev. Lett.* **2014,** *112* (21), 216101.
100. Heverhagen, J.; Tasinkevych, M.; Rahman, A.; Black, C. T.; Checco, A., Slip Length Enhancement in Nanofluidic Flow using Nanotextured Superhydrophobic Surfaces. *Advanced Materials Interfaces* **2016,** *3* (17), 1600303.
101. Mouterde, T.; Lehoucq, G.; Xavier, S.; Checco, A.; Black, C. T.; Rahman, A.; Midavaine, T.; Clanet, C.; Quere, D., Antifogging abilities of model nanotextures. *Nat. Mater.* **2017,** *16* (6), 658-663.
102. Rahman, A.; Ashraf, A.; Xin, H.; Tong, X.; Sutter, P.; Eisaman, M. D.; Black, C. T., Sub-50-nm self-assembled nanotextures for enhanced broadband antireflection in silicon solar cells. *Nat Commun* **2015,** *6*.
103. Liapis, A. C.; Rahman, A.; Black, C. T., Self-assembled nanotextures impart broadband transparency to glass windows and solar cell encapsulants. *Appl. Phys. Lett.* **2017,** *111* (18), 183901.
104. Subramanian, A.; Tiwale, N.; Doerk, G.; Kisslinger, K.; Nam, C.-Y., Enhanced Hybridization and Nanopatterning via Heated Liquid-Phase Infiltration into Self-Assembled Block Copolymer Thin Films. *ACS Applied Materials & Interfaces* **2020,** *12* (1), 1444-1453.
105. Kim, S. Y.; Gwyther, J.; Manners, I.; Chaikin, P. M.; Register, R. A., Metal-Containing Block Copolymer Thin Films Yield Wire Grid Polarizers with High Aspect Ratio. *Adv. Mater.* **2014,** *26* (5), 791-795.
106. Yoo, H. G.; Byun, M.; Jeong, C. K.; Lee, K. J., Performance Enhancement of Electronic and Energy Devices via Block Copolymer Self-Assembly. *Adv. Mater.* **2015,** *27* (27), 3982-3998.
107. Toth, K.; Bae, S.; Osuji, C. O.; Yager, K. G.; Doerk, G. S., Film Thickness and Composition Effects in Symmetric Ternary Block Copolymer/Homopolymer Blend Films: Domain Spacing and Orientation. *Macromol.* **2021,** *54* (17), 7970-7986.
108. Peng, Q.; Tseng, Y.-C.; Darling, S. B.; Elam, J. W., Nanoscopic Patterned Materials with Tunable Dimensions via Atomic Layer Deposition on Block Copolymers. *Adv. Mater.* **2010,** *22* (45), 5129-5133.
109. Ramanathan, M.; Tseng, Y.-C.; Ariga, K.; Darling, S. B., Emerging trends in metal-containing block copolymers: synthesis, self-assembly, and nanomanufacturing applications. *Journal of Materials Chemistry C* **2013,** *1* (11), 2080-2091.
110. Yager, K. G., SciAnalysis. https://github.com/CFN-softbio/SciAnalysis/, 2019.